Quantum Interface for Telecom Frequency Conversion Based on Diamond-Type Atomic Ensembles

Po-Han Tseng[1,*], Ling-Chun Chen[1,2], Jiun-Shiuan Shiu[1,2], and Yong-Fan Chen[1,2]

[1]*Department of Physics, National Cheng Kung University, Tainan 70101, Taiwan*

[2]*Center for Quantum Frontiers of Research & Technology, Tainan 70101, Taiwan*

*E-mail: peter.pohan.tseng@gmail.com

ABSTRACT

In a fiber-based quantum network, quantum frequency conversion (QFC) serves as a pivotal quantum interface for efficiently bridging the frequency gap between atomic quantum devices and telecom fibers. In this study, we explore an efficient telecom-band QFC mechanism based on diamond-type four-wave mixing (FWM) with rubidium energy levels. The mechanism enables the conversion of photons between the near-infrared wavelength of 795 nm and the telecom band of 1367 or 1529 nm. Using the Heisenberg-Langevin approach, we optimize conversion efficiency (CE) across varying optical depths while addressing the applied field absorption loss and present corresponding experimental parameters. Moreover, by employing the reduced-density-operator theory to construct a theoretical framework, we demonstrate that this diamond-type FWM scheme can maintain the quantum characteristics of input photons with high fidelity, such as quadrature variances and photon statistics. Importantly, these properties remain unaffected by vacuum field noise, enabling the system to achieve high-purity QFC. Another significant contribution lies in examining how this scheme impacts quantum information (QI) encoded in photon-number, path, and polarization degrees of freedom (DOFs). These encoded qubits exhibit remarkable entanglement retention under sufficiently high CE and achieve unity fidelity for perfect CE. This comprehensive exploration establishes a theoretical foundation for the application of the diamond-type QFC scheme based on atomic ensembles in quantum networks, laying essential groundwork for advancing the scheme in distributed quantum computing and long-distance quantum communication.

Theoretical Framework

Field Operator

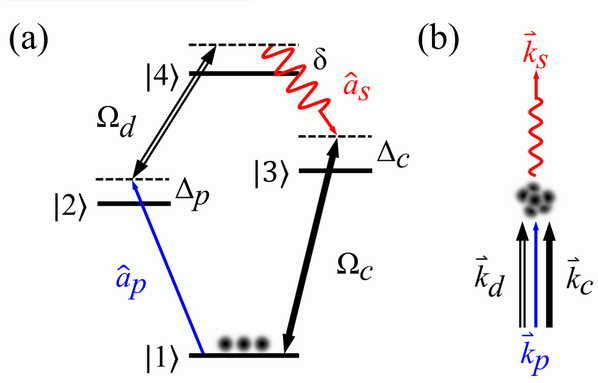

FIG. 1. Diamond-type cold atomic ensemble QFC system. (a) Energy level diagram illustrating the QFC scheme and the corresponding transitions for the four participating fields. (b) Schematic diagram illustrating the propagation directions of the participating fields. All light fields propagate in the same direction, nullifying the phase mismatch in the system. The presented scenario involves frequency down-conversion, where the probe field is transformed into the signal field. Conversely, up-conversion proceeds in the opposite manner, converting the signal field back to the probe field.

We consider a diamond-type FWM system depicted in Fig. 1(a). By utilizing the Heisenberg–Langevin approach [1, 2], we can derive the exact formula of the field operators. The first-order atomic evolution is governed by the following set of Heisenberg–Langevin equations:

$$\frac{\partial}{\partial t}\hat{\sigma}_{12}^{(1)} = i\left[\hat{a}_p g_p \left\langle\hat{\sigma}_{11}^{(0)}\right\rangle + \frac{\Omega_d^*}{2}\hat{\sigma}_{14}^{(1)} - \frac{\Omega_c}{2}\hat{\sigma}_{32}^{(1)} + \Delta_p\hat{\sigma}_{12}^{(1)}\right] - \frac{1}{2}\gamma_{21}\hat{\sigma}_{12}^{(1)} + \hat{F}_{12}, \quad (1)$$

$$\frac{\partial}{\partial t}\hat{\sigma}_{14}^{(1)} = i\left[\hat{a}_s g_s \left\langle\hat{\sigma}_{13}^{(0)}\right\rangle e^{-i\Delta kz} + \frac{\Omega_d}{2}\hat{\sigma}_{12}^{(1)} - \frac{\Omega_c}{2}\hat{\sigma}_{34}^{(1)} + \delta\hat{\sigma}_{14}^{(1)}\right] - \frac{1}{2}\gamma_{41}\hat{\sigma}_{14}^{(1)} + \hat{F}_{14}, \quad (2)$$

$$\frac{\partial}{\partial t}\hat{\sigma}_{32}^{(1)} = i\left[\hat{a}_p g_p \left\langle\hat{\sigma}_{31}^{(0)}\right\rangle + \frac{\Omega_d^*}{2}\hat{\sigma}_{34}^{(1)} - \frac{\Omega_c^*}{2}\hat{\sigma}_{12}^{(1)} + (\Delta_p - \Delta_c)\hat{\sigma}_{32}^{(1)}\right] - \frac{1}{2}\gamma_{32}\hat{\sigma}_{32}^{(1)} + \hat{F}_{32}, \quad (3)$$

$$\frac{\partial}{\partial t}\hat{\sigma}_{34}^{(1)} = i\left[\hat{a}_s g_s \left\langle\hat{\sigma}_{33}^{(0)}\right\rangle e^{-i\Delta kz} + \frac{\Omega_d}{2}\hat{\sigma}_{32}^{(1)} - \frac{\Omega_c^*}{2}\hat{\sigma}_{14}^{(1)} + (\delta - \Delta_c)\hat{\sigma}_{34}^{(1)}\right] - \frac{1}{2}\gamma_{43}\hat{\sigma}_{34}^{(1)} + \hat{F}_{34}. \quad (4)$$

To investigate the evolution of the probe and signal fields propagating in the diamond-type atomic medium, we solve the following Maxwell-Schrödinger equations:

$$\left(\frac{1}{c}\frac{\partial}{\partial t} + \frac{\partial}{\partial z}\right)\hat{a}_p(z,t) = i\frac{N}{c}g_p^*\hat{\sigma}_{12}^{(1)}(z,t), \quad (5)$$

$$\left(\frac{1}{c}\frac{\partial}{\partial t} + \frac{\partial}{\partial z}\right)\hat{a}_s(z,t) = i\frac{N}{c}g_s^*\hat{\sigma}_{34}^{(1)}(z,t)e^{i\Delta kz}, \quad (6)$$

$$\frac{\partial}{\partial z}\Omega_c(z) = \frac{i\alpha_c\Gamma_{31}}{2L}\left\langle\hat{\sigma}_{13}^{(0)}(z)\right\rangle. \quad (7)$$

Since we considered the coupling field absorption loss $\Omega_c(z)$, the field operators in frequency domain must be solved by using the Magnus expansion as follows:

$$\begin{bmatrix}\tilde{a}_p(L,\omega)\\ \tilde{a}_s(L,\omega)\end{bmatrix} = e^{\Omega(L,\omega)}\begin{bmatrix}\tilde{a}_p(0,\omega)\\ \tilde{a}_s(0,\omega)\end{bmatrix} + e^{\Omega(L,\omega)}\sum_{\alpha_i}\int_0^L e^{-\Omega(z,\omega)}\begin{bmatrix}\zeta_{\alpha_i}^p(z,\omega)\\ \zeta_{\alpha_i}^s(z,\omega)\end{bmatrix}\tilde{f}_{\alpha_i}(z,\omega)dz, \quad (8)$$

where the parametric evolution term $e^{\Omega(L,\omega)}$ can be expressed into a 2×2 matrix form explicitly.

Density Operator

The reduced-density-operator approach [1, 3] is employed to establish the connection between the field operators in the Heisenberg picture and the corresponding density operators in the Schrödinger picture. The density matrix element of the converted signal field is obtained as follows:

$$\rho_{s,mn}(L) = \mathrm{tr}\left\{\sum_{l=0}^{\infty}\chi_{mnl}\left[\tilde{a}_s{}^\dagger(L)\right]^{l+n}\left[\tilde{a}_s(L)\right]^{l+m}\rho_i\right\}, \quad (9)$$

where we define $\chi_{mnl} = \frac{(-1)^l}{l!}\frac{1}{\sqrt{n!m!}}$. Through substituting Eq. (8) into Eq. (9) and using the generalized Wick's theorem, explicit form of the converted density matrix element is as follows:

$$\rho_{s,mn}(L) = \sum_{l=0}^{\infty}\chi_{mnl}\,tr_P\left\{\left[C^*(0)\tilde{a}_p{}^\dagger(0)\right]^{l+n}\left[C(0)\tilde{a}_p(0)\right]^{l+m}\rho_p(0)\right\}. \quad (10)$$

Note that the normal-order diffusion coefficients are calculated to be zero under the perturbative probe and signal fields. We extend the theory to explore a QFC scheme comprising N spatially separated atomic ensembles, and the density matrix element of the converted signal field is

$$\rho^s_{m_1\ldots m_N,n_1\ldots n_N}(L) = \sum_{l_1\ldots l_N=0}^{\infty}\chi_{m_1\ldots m_N n_1\ldots n_N l_1\ldots l_N}\,tr_p\left\{\prod_{j=1}^{N}\left[C_j^*\tilde{a}_{p,j}^\dagger(0)\right]^{n_j+l_j}\left[C_j\tilde{a}_{p,j}(0)\right]^{m_j+l_j}\rho_p(0)\right\}. \quad (11)$$

Conversion Efficiency Maximization

Here, we assume that the input field has reached a steady state, thus we focus solely on the single-frequency-mode behavior of the QFC system. The signal (probe) photon number for frequency down-conversion (up-conversion) can be derived as follows:

$$n_{s,\omega}(L) = |C(\omega)|^2\left\langle\tilde{a}_{p,\omega}{}^\dagger(0)\tilde{a}_{p,\omega}(0)\right\rangle + \sum_{\alpha_i,\alpha_j}\int_0^L Q_{\alpha_i}^*(z,\omega)Q_{\alpha_j}(z,\omega)D_{\alpha_i^\dagger,\alpha_j}dz,$$

$$n_{p,\omega}(L) = |B(\omega)|^2\left\langle\tilde{a}_{s,\omega}{}^\dagger(0)\tilde{a}_{s,\omega}(0)\right\rangle + \sum_{\alpha_i,\alpha_j}\int_0^L P_{\alpha_i}^*(z,\omega)P_{\alpha_j}(z,\omega)D_{\alpha_i^\dagger,\alpha_j}dz,$$

where the normal-order diffusion coefficients $D_{\alpha_i^\dagger,\alpha_j}$ are calculated to be zero. The general formula of CE for down- and up-conversion are as follows:

$$\eta_d = \frac{n_{s,0}(L)}{n_{p,0}(0)} = |C(0)|^2,\ \eta_u = \frac{n_{p,0}(L)}{n_{s,0}(0)} = |B(0)|^2.$$

We plot the optimized CE curve for frequency down-conversion using a ^{87}Rb atomic ensemble, as shown in Fig. 2 (up-conversion yields the same result).

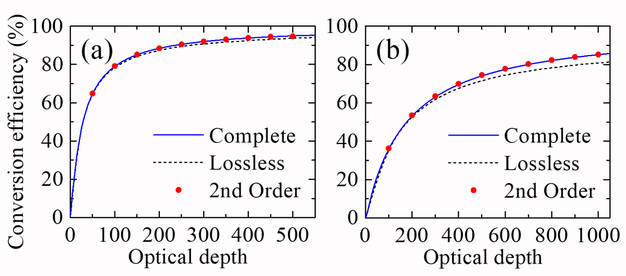

FIG. 2. Optimized CE is presented as a function of OD in the blue solid curve for both (a) telecom E-band QFC scheme and (b) telecom C-band QFC scheme. The black dotted curves show the CE curves for the model without considering the coupling field absorption loss.

- The transition schemes are carefully selected to ensure a cycling transition between $|1\rangle$ and $|3\rangle$ and that the CE is maximized among all possible energy level configurations.
- We emphasize the contribution of coupling field absorption loss is non-negligible.
- The optimized parameters corresponding to the optimized CE in Fig. 2 are all experimentally attainable, and these optimization results can also be carried out using ^{85}Rb.

Quantum Characteristics

Quadrature Variances

We derived the general formulas for the quadrature variances of the converted field in both the down- and up-conversion cases, which are as follows:

$$\mathrm{var}\left[X'_{s(p)}(L)\right] = \eta_{d(u)}\mathrm{var}\left[X_{p(s)}(0)\right] + \tfrac{1}{4}\left(1-\eta_{d(u)}\right),$$

$$\mathrm{var}\left[Y'_{s(p)}(L)\right] = \eta_{d(u)}\mathrm{var}\left[Y_{p(s)}(0)\right] + \tfrac{1}{4}\left(1-\eta_{d(u)}\right).$$

The converted quadrature variances for some specific input fields are depicted in Fig. 3.

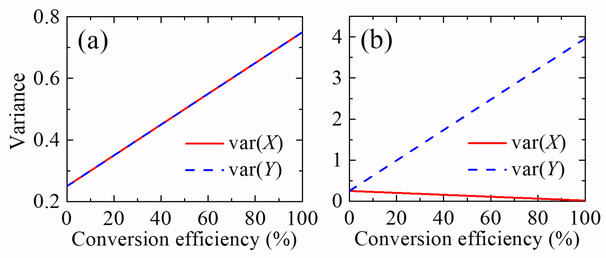

FIG. 3. Quadrature variances are analyzed as a function of CE for the input field in (a) the single-photon Fock state or (b) the 6-dB squeezed coherent state.

Photon Statistics

The converted quantum state for Fock and coherent input fields are derived explicitly by using Eq. (10). For input a single-photon Fock state $|1\rangle$, the density operator of the converted field is as follows:

$$\rho_{s(p)}(L) = \left(1-\eta_{d(u)}\right)|0\rangle\langle 0| + \eta_{d(u)}|1\rangle\langle 1|.$$

For input a coherent state $|\beta\rangle$, the converted state is

$$|\psi_{s(p)}(L)\rangle = \left|\sqrt{\eta_{d(u)}}\beta\right\rangle.$$

The conversion fidelity is depicted in Fig. 4.

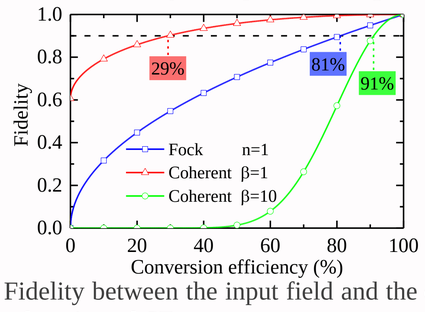

FIG. 4. Fidelity between the input field and the converted field as a function of CE.

Quantum Interface

Qubit Retention

Here we demonstrate how the QFC scheme retain a single qubit encoded in various DOFs with $\rho_p(0) = \begin{bmatrix}\rho_{00} & \rho_{01}\\ \rho_{10} & \rho_{11}\end{bmatrix}$.

DOF:	**Single-Rail**	**Path**	**Polarization**
logical basis:	$\lvert n=0\rangle, \lvert n=1\rangle$	$\lvert 1\rangle_D\lvert 0\rangle_U, \lvert 0\rangle_D\lvert 1\rangle_U$	$\lvert 1_H 0_V\rangle, \lvert 0_H 1_V\rangle$
converted qubit:	$\begin{bmatrix}\rho_{00}+(1-\eta_d)\rho_{11} & \sqrt{\eta_d}\rho_{01}\\ \sqrt{\eta_d}\rho_{10} & \eta_d\rho_{11}\end{bmatrix}$	$\begin{bmatrix}\eta_D\rho_{00} & \sqrt{\eta_D\eta_U}\rho_{01}\\ \sqrt{\eta_U\eta_D}\rho_{10} & \eta_U\rho_{11}\end{bmatrix}$	$\begin{bmatrix}\eta_D\rho_{00} & \sqrt{\eta_D\eta_U}\rho_{01}\\ \sqrt{\eta_U\eta_D}\rho_{10} & \eta_U\rho_{11}\end{bmatrix}$

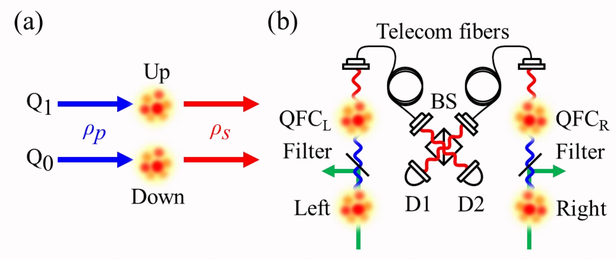

FIG. 5. Schematic diagram depicting the QFC scheme for path-encoded qubits integrated with the DLCZ protocol. (a) Frequency down-conversion of a path-encoded qubit. (b) The integration with the DLCZ protocol.

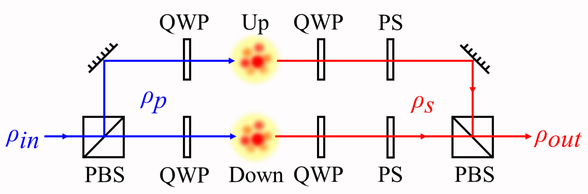

FIG. 6. QFC scheme for a polarization-encoded qubit. The polarization beam splitter (PBS) convert the photon between path and polarization DOFs. Quarter-wave plates (QWPs) are used to met the requirements of the optimized QFC scheme.

Entanglement Retention

We utilize Eq. (11) to discuss the QFC involving an arbitrary number of entangled qubits (N-qubit QFC).

$$\rho^s_{m_1\ldots m_N,n_1\ldots n_N}(L) = \sum_{q_1\ldots q_N=0}^{1}\sum_{r_1\ldots r_N=0}^{1}\rho^p_{q_1\ldots q_N,r_1\ldots r_N}(0)$$

$$\times\prod_{j=1}^{N}\left\{\delta_{m_j n_j,00}\left[\delta_{q_j r_j,00} + \delta_{q_j r_j,11}\left(1-\eta_j\right)\right] + \delta_{m_j n_j,01}\delta_{q_j r_j,01}C_j^* + \delta_{m_j n_j,10}\delta_{q_j r_j,10}C_j + \delta_{m_j n_j,11}\delta_{q_j r_j,11}\eta_j\right\}.$$

The qubits reach unity fidelity for perfect CE, indicating the QFC scheme as a robust quantum interface.

Polarization-entangled EPR pair after the QFC:

- Input state $|\Phi^+\rangle = \frac{1}{\sqrt{2}}\left(|0_1 0_2\rangle + |1_1 1_2\rangle\right)$, where $|0\rangle \equiv |1_H 0_V\rangle$ and $|1\rangle \equiv |0_H 1_V\rangle$.
- Coincidence detection probability $P_c = \frac{\bar{\eta}_A^2+\bar{\eta}_B^2}{2}$.
- Post-selected fidelity $F = \frac{\bar{\eta}_A+\bar{\eta}_B}{\sqrt{2(\bar{\eta}_A^2+\bar{\eta}_B^2)}}$.

Violation of CHSH Bell inequality $|S| \le 2$:

$$S = 2\sqrt{2}F^2 > 2, F > 2^{-1/4} \approx 84.1\%.$$

The conversion processes exhibiting quantum nonlocality is depicted in Fig. 7(b).

Similar results can be obtained for other Bell state, such as $|\Phi^-\rangle$, $|\Psi^+\rangle$, and $|\Psi^-\rangle$.

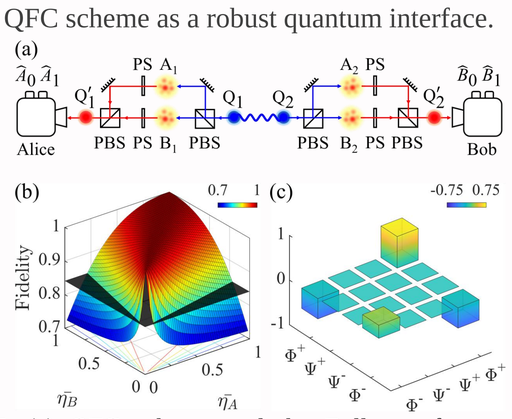

FIG. 7. (a) QFC scheme and the Bell test for a pair of polarization-entangled qubits Q_1 and Q_2. (b) The post-selected fidelity. (c) The converted density operator with F=$2^{-1/4}$.

Conclusion

- We optimize CE across varying optical depths within experimentally attainable conditions, taking into account the non-negligible practical field absorption loss scenarios.
- The diamond-type QFC scheme can maintain the quantum characteristics of input photons with high fidelity, such as quadrature variances and photon statistics.
- We demonstrate the robust preservation of entangled qubits encoded in the photon-number, path, and polarization DOFs, revealing the ability of the frequency converter as a quantum interface.
- The CE and fidelity of QI remain unaffected by vacuum field noise, enabling high-purity QFC using the diamond-type atomic ensembles.

REFERENCES

[1] P.-H. Tseng, L.-C. Chen, J.-S. Shiu, and Y.-F. Chen, Phys. Rev. A **109**, 043716 (2024).

[2] P. Kolchin, Phys. Rev. A **75**, 033814 (2007).

[3] F. Kheirandish, Eur. Phys. J. Plus **135**, 243 (2020).